Journal of Theoretical Biology 435 (2017) 184–198

Contents lists available at ScienceDirect

Journal of Theoretical Biology

journal homepage: www.elsevier.com/locate/jtbi

# Optimal construction of army ant living bridges

Jason M. Graham[a,d,1,*], Albert B. Kao[b,1], Dylana A. Wilhelm[c,d], Simon Garnier[d]

[a] Department of Mathematics, University of Scranton, USA
[b] Department of Organismic and Evolutionary Biology, Harvard University, USA
[c] Department of Mathematics and Statistics, James Madison University, USA
[d] Department of Biological Sciences, New Jersey Institute of Technology, USA

ARTICLE INFO

*Article history:*
Received 14 March 2017
Revised 1 September 2017
Accepted 18 September 2017
Available online 20 September 2017

*Keywords:*
Swarm intelligence
Collective behavior
Army ants
Optimality
Self-assembly

ABSTRACT

Integrating the costs and benefits of collective behaviors is a fundamental challenge to understanding the evolution of group living. These costs and benefits can rarely be quantified simultaneously due to the complexity of the interactions within the group, or even compared to each other because of the absence of common metrics between them. The construction of 'living bridges' by New World army ants – which they use to shorten their foraging trails – is a unique example of a collective behavior where costs and benefits have been experimentally measured and related to each other. As a result, it is possible to make quantitative predictions about when and how the behavior will be observed. In this paper, we extend a previous mathematical model of these costs and benefits to much broader domain of applicability. Specifically, we exhibit a procedure for analyzing the optimal formation, and final configuration, of army ant living bridges given a means to express the geometrical configuration of foraging path obstructions. Using this procedure, we provide experimentally testable predictions of the final bridge position, as well as the optimal formation process for certain cases, for a wide range of scenarios, which more closely resemble common terrain obstacles that ants encounter in nature. As such, our framework offers a rare benchmark for determining the evolutionary pressures governing the evolution of a naturally occurring collective animal behavior.



## 1. Introduction and background

Over the past four decades, studies have revealed the functional consequences of collective animal behaviors, which are often driven by interactions between individuals with little or no global knowledge (Camazine et al., 2001; Couzin, 2009; Couzin and Krause, 2003; Garnier et al., 2007; Sumpter, 2010). The cohesive movement of bird flocks and fish schools, some of the most visually striking examples of how animal groups can dynamically self-organize, can allow for improved migration accuracy (Guttal and Couzin, 2010), predator avoidance (Wolf et al., 2013), and resource finding (Couzin et al., 2005). However, collective behavior also operates at less conspicuous, but equally functionally important, scales in order to generate division of labor (Duarte et al., 2011), pattern formation (Detrain and Deneubourg, 2006; Theraulaz et al., 2002), or physical construction (Buhl et al., 2005; King et al., 2015) across many animal taxa.

One of the principal challenges in studying collective behavior is simultaneously quantifying both the benefits and costs associated with group living in order to understand the overall selective pressure on the behavior and hence its evolution. In some cases, the benefits, such as the improvements in navigation (Berdahl et al., 2013), or the costs, such as an increase in the risk of disease (Cross et al., 2010), have been measured in isolation. However, since the proximate currencies of fitness related to benefits and costs can be very different (*e.g.*, navigation direction and disease risk), and operate at different spatial or temporal scales, it is often difficult to measure both benefits and costs simultaneously in order to estimate the ultimate fitness consequences of group living.

The construction of living bridges by the army ant *Eciton hamatum* is a unique example of a collective behavior that is amenable to measurements of both costs and benefits (Reid et al., 2015). Therefore, it allows for quantitative predictions about when and how the behavior will be observed. Found in the tropical forests of Central and South America, army ants are nomadic, moving their entire colony (sometimes exceeding a million individuals) to a new location each day in search of new sources of food while the colony has developing young (Rettenmeyer, 1963; Schneirla, 1945; 1972). As a consequence of this nomadic lifestyle, these ants –

* Corresponding author.
*E-mail address:* jason.graham@scranton.edu (J.M. Graham).
[1] The authors contributed equally to this work.

https://doi.org/10.1016/j.jtbi.2017.09.017
0022-5193/

unlike most other ants – face severe time constraints when generating new foraging routes each day. While ants living in a permanent nest site can thoroughly explore their environment (Deneubourg et al., 1990; Devigne and Detrain, 2002) or clear trails of vegetation (Bochynek et al., 2016; Bruce and Burd, 2012; Howard, 2001; Kost et al., 2005) in order to create relatively straight and efficient foraging paths, army ant trails often weave tortuously through the complex tropical forest floor (Schneirla, 1972; Solé et al., 2000).

In order to improve the efficiency of their trails, army ants are capable of linking their own bodies together to dynamically create physical structures along the foraging path (Anderson et al., 2002; Garnier et al., 2013; Reid et al., 2015; Rettenmeyer, 1963; Schneirla, 1972). These structures may be used to widen paths to increase the flux of ants, or to form bridges over gaps in the terrain (reaching spans of over 12 cm, or approximately 12 ant body lengths) to decrease the tortuosity of their trails (Powell and Franks, 2007; Reid et al., 2015). Moreover, Powell and Franks (2007) showed that these structures allow prey-laden ants to move at maximum speed on the trail, as if they were walking on a flat surface. Ants modulate their bridge-building behavior in response to local information, allowing these bridges to adapt to current traffic conditions, recover from damage, and dissemble when underused (Garnier et al., 2013), so that they exist as needed at particular points along the trail.

While the living bridges can increase the flow of ants and resources along trails, they also impose a cost on the colony. The ants forming the bridges are locked into the structure, sometimes for several minutes at a time (Garnier et al., 2013), preventing them from participating in other foraging activities such as capturing and killing prey or transporting food items along the trail. Understanding the overall effect of these living structures on the colony's foraging rate requires a quantification of both the benefit (shortening the travel distance) and cost (removing ants from the foraging pool) of each structure, and converting these to the common currency of overall foraging rate.

In a recent study, Reid et al. (2015) experimentally manipulated living bridges built by colonies of *E. hamatum* and measured these benefits and costs. The researchers inserted deviations into existing foraging trails (Fig. 1) and recorded the formation of bridges on the experimental apparatus. They showed that bridges initiated at the bend of the deviation but over time grew and moved away from the initiation point to increasingly shortcut the deviation (Fig. 2). However, the final, steady state, position of the bridges tended to not fully minimize the trail length. Instead, the distance that the bridge traveled, and hence the benefit (trail shortening) derived from the living bridge, depended on the angle of the apparatus deviation (Reid et al., 2015). To measure the cost of the bridge to the colony, Reid et al. (2015) estimated the number of ants required to maintain a bridge of a certain length by measuring the surface area of the bridge (which is an appropriate approximation because bridges consist of a monolayer of ants). Crucially, the bridges were observed to widen as they lengthened, so that while the travel distance saved increased linearly with bridge length, the number of ants diverted from the foraging pool increased quadratically with bridge length.

The researchers converted the change in travel distance and the change in the number of available foraging ants caused by the construction of a bridge into an overall change in the local density of foraging ants on the trail. This served as a proxy for the trail foraging rate and provided a common currency with which to directly compare the costs and benefits of a given living bridge. We note that this assumes that army ants do not recruit workers at the bivouac to compensate for ants locked in the bridge structure. However, this assumption is reasonable since such density-driven recruitment would not be trivial to achieve for the ants. An army ant trail can sometimes reach several hundred meters and density can vary enormously along the trail based on the local conditions (*e.g.* because of terrain configuration). Individual ants would therefore have to integrate density information over a long enough portion of the trail before making the decision to walk back a sometime long distance toward the bivouac (a time during which density on the trail might change). Maximizing the trail foraging rate (density of foraging ants) as a function of bridge position led to a unique, non-trivial, optimal position, which the researchers showed could be matched closely to the empirically observed bridge positions (Reid et al., 2015).

(a)

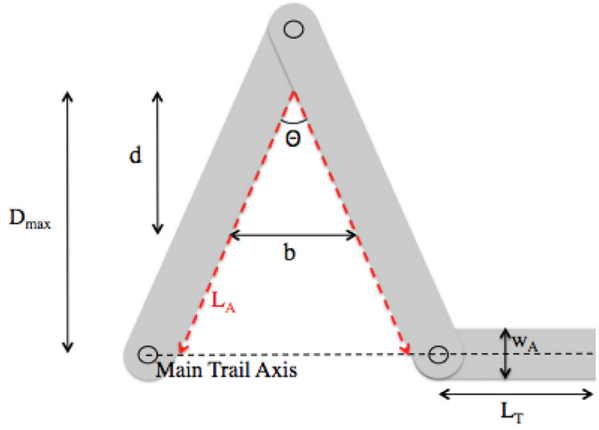


(b)

**Fig. 1.** (a) Field apparatus used in Reid et al. (2015) to experimentally manipulate living bridges built by colonies of army ant *Eciton hamatum*. (b) Schematic representation of the experimental apparatus introduced into a foraging trail of army ants in Reid et al. (2015). The introduction of such an apparatus has the effect of adding an additional length $L_A$ to the distance ($L_T$) foraging ants must travel. In order to shortcut this additional distance, army ants construct a living bridge that initially forms at an apex of angle $\theta$, and moves down toward the main trail axis until reaching some optimal position. Here $w_A$ is the width of an apparatus arm.

Here, we propose to broaden the domain of applicability of the mathematical model introduced by Reid et al. (2015). We do so by demonstrating a procedure that can be applied to make predictions regarding both the growth trajectory, as well as the final stable position, of living bridges for a much wider range of geometrical scenarios along a trail. We first recapitulate quantitatively the costs and benefits of living bridges and describe the procedure for identifying the growth and final configuration of the bridge (or bridges) that is predicted to maximize foraging rate. Then, we apply this process to scenarios with asymmetric obstacles and with multi-

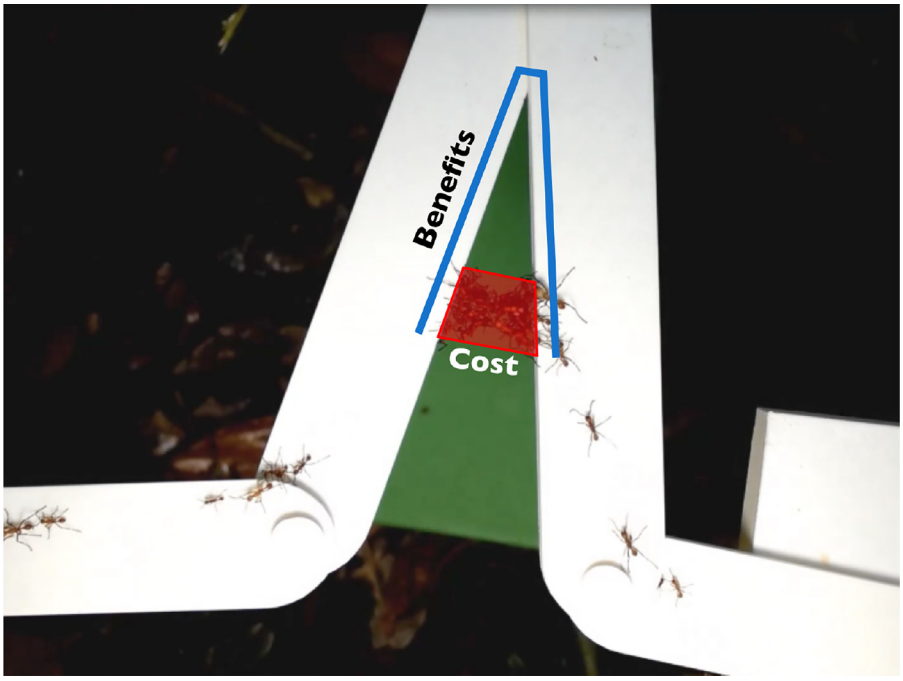


**Fig. 2.** Field apparatus used in Reid et al. (2015) to experimentally manipulate living bridges built by colonies of army ant *Eciton hamatum*. This figure shows the formation of a living bridge together with an illustration of the cost-benefit relationship studied in Reid et al. (2015).

ple consecutive obstacles, which we argue represent the building blocks necessary for modeling most scenarios that army ants encounter in nature.

These predictions, as well as others that can be generated with our framework, can be used to further test empirically the hypothesis that army ant living bridges serve to maximize foraging rate along trails. The predictions include the number of bridges, their position relative to the apparatus (or natural obstacle) and to other bridges, and their angle relative to the main foraging trail, which can be directly measured in field experiments. In addition to lending themselves to hypothesis testing, the scenarios considered here resemble more closely obstacles that are typically encountered by army ants, potentially allowing for a more complete understanding of bridge building dynamics by army ants in nature.

## 2. Methods

### 2.1. Cost-benefit framework

As in Reid et al. (2015), we consider a foraging trail of total length $L_T$ and $N$ army ants. If an experimental apparatus (or natural obstacle) is introduced to the trail, then this adds an additional length of $L_A$ to the distance over which the ants must travel (Fig. 1). Thus, in the absence of any bridges the overall foraging density of ants is

$$\frac{\text{Number of ants}}{\text{Total distance}} = \frac{N}{L_T + L_A}. \tag{1}$$

The magnitude of the length $L_A$ depends on the geometric configuration of the apparatus as well as our assumption that ant trails tend to follow the inner edge of the apparatus in order to minimize travel distance (see Reid et al., 2015 and below). The trail length $L_T$ is fixed. We estimate the number of ants $N$ by multiplying the mean empirically measured density of foraging ants by $L_T + L_A$, as in Reid et al. (2015).

The presence of one (or more) bridges will modify both the number of ants moving on the trail (since the bridges are comprised of ants) and the distance of travel, both of which will modulate the traffic density on the trail. The number of available foraging ants becomes $N$ minus the number of ants sequestered in the bridge structures $n_b$, *i.e.*,

$$N - n_b. \tag{2}$$

However, there are substantial functional differences between a typical bridge-building and non-bridge-building (*i.e.*, foraging) ant. Ants that take up positions in bridges tend to be smaller and less effective at capturing and carrying prey items (Powell and Franks, 2005; 2006). Therefore, if our unit of ants is assumed to be foraging ants, then the cost of including a (smaller) ant into the bridge structure will actually be less than one foraging ant. In order to account for these size and functional differences between bridge-building and foraging ants, we introduce a free parameter $\alpha$ and modify Eq. (2) to become

$$N - \frac{n_b}{\alpha}, \tag{3}$$

where we set $\alpha = 17.02$ as in Reid et al. (2015). The value of this parameter may need to be refit when testing new ecological conditions, such as nighttime colony migrations, where the functional differences between ants of different sizes may not be the same as when foraging.

In the presence of bridges, we assume that the distance of travel for the foraging ants, $f$, is the shortest path through the apparatus-bridge complex. Thus, the density function to be optimized is

$$\rho = \frac{N - n_b/\alpha}{f}. \tag{4}$$

Note that we choose here to conduct the optimization over the size of the experimental apparatus, rather than the total trail length. In Reid et al. (2015), it is estimated that there is between one and ten bridges per meter of trail on a typical army ant trail (depending on terrain configuration and traffic intensity). This corresponds to an average of one bridge every 20–30 cm, which is approximately the length of the apparatus in Reid et al. (2015). Therefore, conducting the optimization over the length of the apparatus should be

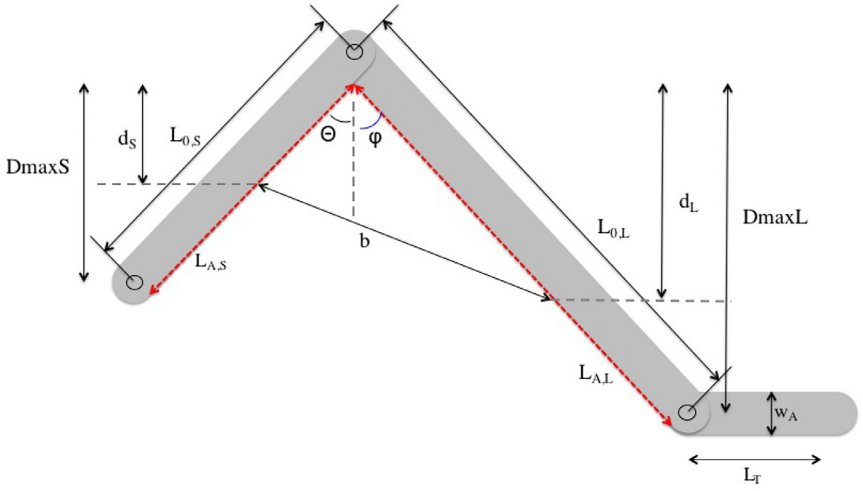


**Fig. 3.** Schematic of a theoretical apparatus that is predicted to result in the construction of army ant living bridges that are not necessarily parallel to the main trail axis. The additional length of such an apparatus added to the path of travel is $L_{A,S} + L_{A,L}$. Here $w_A$ is the width of an apparatus arm. All other variables and parameters are described in Tables 1 and 2.

equivalent to conducting it over the total trail length. In addition, with around 10 ants sequestered in each bridge, and depending on colony size, the Reid et al. (2015) estimate indicates that the total number of ants sequestered in bridges would occupy between 2 and 20% of the total colony population. This is a significant cost for the colony that is compensated by a significant increase in foraging efficiency, which was estimated by Powell and Franks (2007) as an up to 79% higher daily prey intake in comparison to a no-bridge situation. In order to maximize the density of foraging ants for a particular geometric configuration of apparatuses (or obstacles in nature), all that is left is to describe how the number of ants in the bridge $n_b$ and trail length $f$ vary with bridge position.

## 2.2. Procedure for predicting optimal bridges

### 2.2.1. Finding the globally optimal bridge configuration

The configuration of a bridge is described exactly by where its two ends attach to the apparatus. Because the ends of the bridges must connect to the experimental apparatus (or some other physical substrate), the apparatus constrains the range of possible configurations that a bridge can have. For apparatuses (or other obstacles), a bridge end can attach anywhere from the apex of the deviation to the end of the apparatus arm (or obstacle). If we denote the apex as distance 0 and the ends of the two apparatus arms as $D_{\max,1}$ and $D_{\max,2}$, then the possible configurations of the bridge are contained within the rectangle $[0, D_{\max,1}] \times [0, D_{\max,2}]$. For scenarios with multiple deviations, we assume that one bridge can form for each apex present, so for a scenario with $A$ apexes, we search within the $2A$ dimensional hyperrectangle to locate the optimal bridge configuration. we carried out this optimization via numerical routines using the R package DEoptim (Ardia et al., 2011a; 2011b; 2015; Mullen et al., 2011; Price et al., 2006).

For each possible configuration of bridges, we need to be able to calculate the number of ants sequestered and the distance that foraging ants have to traverse. For a given configuration, the lengths of the bridges can be directly calculated. Then, following the results of Reid et al. (2015), we assume that the width of a bridge increases linearly as the bridge get longer. With this assumption, the surface area of a bridge can be computed for any bridge configuration, and the number of ants comprising a bridge estimated by further assuming each ant has a typical length and width.

To calculate the distance that foraging ants have to traverse given a certain configuration of bridges, we assume that ants make the following journey: starting from the main foraging trail, they travel up the inner edge of the first apparatus arm until the first bridge is encountered, cross the first bridge along the middle, travel along the second apparatus arm from the first bridge to the second bridge, cross the second bridge, and so on until the end of the apparatus has been reached. In short, we assume that ants take the shortest possible path through the apparatus-bridge complex.

### 2.2.2. Finding the optimal growth trajectory

If there is a selective pressure on the final bridge position to maximize the foraging rate, then there should also be pressure to maximize foraging rate during the bridge construction process. With this assumption, we can predict the growth trajectory that a bridge takes to reach the final configuration.

To do so, we fix the total length of all bridges in the structure to be a certain length. Then, we search this reduced space of possible configurations and locate the configuration that maximizes foraging rate for that bridge length. By setting the length to vary from 0 to the sum of the final optimal lengths, we generate a trajectory that maximizes foraging rate throughout the building process.

When there are multiple bridges within a structure, we reason that during the construction process, each bridge should be the same length for as long as possible. As described above, for apparatuses with arms that are straight, the distance saved from a bridge scales linearly with bridge length, while the number of ants sequestered scales quadratically. Therefore, for a fixed total bridge length, it is optimal for each bridge to be the same length. With this argument, we predict that each bridge will grow at the same rate, until a bridge reaches its optimal position, when it will stop growing while the other bridges continue to grow.

### 2.2.3. Further generalizations

In this framework, we assume that the apparatus (or natural obstacle) consists of a series of straight paths. If this is not the case (*i.e.,* the arms are curved), then some of the assumptions that we made may not hold. For example, it is possible in such scenarios that while growing from an apex, a bridge may get stuck at a local maximum before reaching the globally optimal configuration. A slightly modified procedure would be necessary if generating predictions for these kinds of obstacles.

However, we argue that such scenarios will be rare in nature. In the tropical forest floor, the physical substrate on which bridges

are built will typically be fallen tree branches, which are relatively straight, especially at the spatial scale of army ant bridges (1–10 cm). Obstacles usually consist of overlapping branches, so that the scenarios that we have solved here, including asymmetric obstacles and multiple consecutive obstacles, should form the basic building blocks of the majority of obstacles that army ants encounter in nature. These building blocks can be combined, for example to create multiple asymmetric obstacles, to create increasingly complex challenges.

### 2.3. Asymmetric scenario

#### 2.3.1. Optimal bridge position

We generalize the model described in Reid et al. (2015) by allowing for a difference in the orientations of the two arms of the apparatus relative to the main trail axis, as well as a difference between the lengths of each arm of the apparatus (Fig. 3).

Let $\theta$ and $\phi$ be the angles that the shorter and longer arms (the left and right arms in Fig. 3) respectively make relative to the line perpendicular to the main trail axis, and $L_{0,S}$ and $L_{0,L}$ be the hinge-to-hinge distance along the shorter and longer arms of the apparatus. Then, from purely geometric considerations, the inner length of each arm from the apex of the apparatus to the unconnected end of each arm is

$$L_{A,S} = L_{0,S} - \frac{w_A}{2}\cot\left(\frac{\theta+\phi}{2}\right), \tag{5}$$

$$L_{A,L} = L_{0,L} - \frac{w_A}{2}\cot\left(\frac{\theta+\phi}{2}\right), \tag{6}$$

where $w_A$ is the width of the apparatus arm. Thus, the distance along the apparatus that ants must travel when there is no bridge is $L_A = L_{A,S} + L_{A,L}$.

The maximum possible vertical distance that each end of a bridge could travel down the shorter and longer arm, before the end of each respective arm is reached, is

$$D_{\max,S} = L_{A,S}\cos(\theta), \tag{7}$$

$$D_{\max,L} = L_{A,L}\cos(\phi). \tag{8}$$

If the ends of a particular bridge travel down the shorter and longer arms of the apparatus a vertical distance of $d_S$ and $d_L$, respectively, then according to the law of cosines, the length of the bridge will be

$$b^2 = \left(\frac{L_{A,S}}{D_{\max,S}}d_S\right)^2 + \left(\frac{L_{A,L}}{D_{\max,L}}d_L\right)^2 - 2d_S d_L\frac{L_{A,S}L_{A,L}\cos(\theta+\phi)}{D_{\max,S}D_{\max,L}}, \tag{9}$$

(all parameters and variables used in this model are listed and described in Tables 1 and 2). The total distance of travel for foraging ants through an apparatus with such a bridge is

$$f = L_T + L_A + b - \frac{L_{A,S}}{D_{\max,S}}d_S - \frac{L_{A,L}}{D_{\max,L}}d_L, \tag{10}$$

and we obtain our density function

$$\rho = \frac{N - \frac{n_b}{\alpha}}{f}, \tag{11}$$

where the number of ants sequestered for the formation of a bridge is

$$n_b = \frac{w_\Omega\left(1 - w_\Omega\tan\left(\frac{\theta+\phi}{2}\right)\right)}{l_n w_n}b^2, \tag{12}$$

where $l_n$ and $w_n$ represent the length and width of a typical sequestered bridge ant, and $w_\Omega$ is ratio between the width and length of a living bridge.

To locate the optimal bridge position, we maximize foraging ant density as a function of the bridge end positions $d_S$ and $d_L$, for given values of apparatus angles $\theta$ and $\phi$.

#### 2.3.2. Optimal bridge formation process

Let $b_f$ represent the bridge length parameter, which is to be varied from 0 to the final optimal length. When $b_f$ is fixed, through Eqs. (9)–(11) we arrive at a constrained optimization problem. That is, we seek to optimize the density

$$\rho = \frac{N - \frac{n_{b_f}}{\alpha}}{f}, \tag{13}$$

subject to the constraint

$$b_f^2 = \left(\frac{L_{A,S}}{D_{\max,S}}d_S\right)^2 + \left(\frac{L_{A,L}}{D_{\max,L}}d_L\right)^2 - 2d_S d_L\frac{L_{A,S}L_{A,L}\cos(\theta+\phi)}{D_{\max,S}D_{\max,L}}, \tag{14}$$

where

$$f = L_T + L_A + b_f - \frac{L_{A,S}}{D_{\max,S}}d_S - \frac{L_{A,L}}{D_{\max,L}}d_L, \tag{15}$$

and

$$n_{b_f} = \frac{w_\Omega\left(1 - w_\Omega\tan\left(\frac{\theta+\phi}{2}\right)\right)}{l_n w_n}b_f^2. \tag{16}$$

We note that since $b_f$ is fixed, $n_{b_f}$ and hence $N - \frac{n_{b_f}}{\alpha}$ are now held constant. The values for $L_{A,S}$, $L_{A,L}$, $D_{\max,S}$ and $D_{\max,L}$ are obtained as before.

In the appendix, we derive the values of $d_S$ and $d_L$ in the intervals $[0, D_{\max,S}]$ and $[0, D_{\max,L}]$ respectively that maximize Eq. (13) subject to the constraint given by Eq. (14).

### 2.4. Multiple obstacles scenario

In this model, we consider multiple, symmetric, deviations from the trail. We predict that this scenario may produce multiple bridges that coordinate in a striking fashion, since the position of one bridge may constrain the possible positions of downstream bridges. Figs. 4 and 5 illustrate apparatuses that could be expected to lead to the formation of two and three bridges, respectively.

For the two bridge case illustrated in Fig. 4, let $L_0$ be the hinge-to-hinge length along each of the three segments of the apparatus. Then the inner distance from the apex to the end of each arm is

$$L_{A_1} = L_{A_2} = L_{A_3} = L_0 - \frac{w_A}{2}\cot\left(\frac{\theta}{2}\right), \tag{17}$$

so $L_A = L_{A_1} + L_{A_2} + L_{A_3} = 3L_{A_1}$, and the maximum vertical distance each bridge can travel is

$$D_{\max} = \frac{L_A}{3}\cos\left(\frac{\theta}{2}\right). \tag{18}$$

Then, our density function will take the form

$$\rho = \frac{N - \frac{n_{b_1}}{\alpha} - \frac{n_{b_2}}{\alpha}}{f}, \tag{19}$$

where the number of ants sequestered in each bridge is

$$n_{b_i} = \frac{w_\theta\left(1 - w_\theta\tan\left(\frac{\theta}{2}\right)\right)}{l_n w_n}b_i^2, \quad i = 1, 2, \tag{20}$$

and the length of each bridge is

$$b_i = 2d_i\tan\left(\frac{\theta}{2}\right), \quad i = 1, 2. \tag{21}$$

**Table 1**
Fixed parameters used in all models.

| Notation | Description | Value | Units |
|---|---|---|---|
| $L_T$ | Trail length without bridges | 100 | cm |
| $l_n$ | Length of an average ant when occupying a position within the bridge structure | 0.691 | cm |
| $w_n$ | Width of an average ant when occupying a position within the bridge structure | 0.107 | cm |
| $w_A$ | Width of apparatus arm | 3.3 | cm |
| $\alpha$ | Free parameter to adjust the space occupied by an ant on the trail | 17.02 | |

**Table 2**
Geometric parameters and variables corresponding to asymmetric model representing an apparatus such as shown in Fig. 3.

| Notation | Description | Value | Units |
|---|---|---|---|
| $L_{S,0}$ | Hinge-to-hinge length of left apparatus arm | 22 | cm |
| $L_{L,0}$ | Hinge-to-hinge length of right apparatus arm | 44 | cm |
| $\theta$, $\phi$ | Angle of left and right arm respectively from the vertical | 0 to 45 | degrees |
| $w_\Omega$ | Ratio between width and length of a bridge, value from Reid et al. (2015) | $4.799(\theta+\phi)^{-0.5014}$ | N/A |
| $L_{A,S}$ | Travel length along left arm from apex to opposite hinge | $L_{S,0}-\frac{w_A}{2}\cot\left(\frac{\theta+\phi}{2}\right)$ | cm |
| $L_{A,L}$ | Travel length along right arm from apex to opposite hinge | $L_{L,0}-\frac{w_A}{2}\cot\left(\frac{\theta+\phi}{2}\right)$ | cm |
| $L_A$ | Sum of travel lengths along each arm | $L_{A,S}+L_{A,L}$ | cm |
| $D_{\max,1}$ | Maximum vertical distance from apex to bottom of left arm | $L_{A,S}\cos(\theta)$ | cm |
| $D_{\max,2}$ | Maximum vertical distance from apex to bottom of right arm | $L_{A,L}\cos(\phi)$ | cm |
| $d_1$ | Vertical distance of bridge from apex to position on left arm | 0 to $D_{\max,1}$ | cm |
| $d_2$ | Vertical distance of bridge from apex to position on right arm | 0 to $D_{\max,2}$ | cm |

**Table 3**
Geometric parameters and variables corresponding to two-apex apparatus such as shown in Fig. 4.

| Notation | Description | Value | Units |
|---|---|---|---|
| $L_0$ | Hinge-to-hinge length of each arm | 22 | cm |
| $\theta$ | Angle of each apex | 0 to 60 | degrees |
| $w_\theta$ | Ratio between width and length of a bridge, value from Reid et al. (2015) | $4.799\theta^{-0.5014}$ | N/A |
| $L_{A_1}$, $L_{A_2}$, $L_{A_3}$ | Travel length along each arm of apparatus from apex to opposite hinge | $L_0-\frac{w_A}{2}\cot\left(\frac{\theta}{2}\right)$ | cm |
| $L_A$ | Sum of travel lengths along each arm | $L_{A_1}+L_{A_2}+L_{A_3}$ | cm |
| $D_{\max}$ | Maximum vertical distance from apex to end of each arm | $\frac{L_A}{3}\cos\left(\frac{\theta}{2}\right)$ | cm |
| $d_1$ | Vertical distance of bridge from apex to position on arms forming first apex | 0 to $D_{\max}$ | cm |
| $d_2$ | Vertical distance of bridge from apex to position on arms forming second apex | 0 to $D_{\max}$ | cm |

The length of a trail on an apparatus with two bridges will be

(length of distance along arm 1 - savings from bridge 1)
+ bridge 1
+ distance along arm 2 between bridges + bridge 2
+ (length of distance along arm 3 - savings from bridge 2). (22)

Thus, we have

$$f = L_T + \left(1-\frac{d_1}{D_{\max}}\right)L_{A_1} + \left(1-\frac{d_2}{D_{\max}}\right)L_{A_3} + \left|\frac{D_{\max}-d_1}{\cos\left(\frac{\theta}{2}\right)} - \frac{d_2}{\cos\left(\frac{\theta}{2}\right)}\right| + b_1 + b_2, \quad (23)$$

where all of the parameters are listed and described in Tables 1 and 3.

Putting the last four equations together gives a complete expression for the density as a function of the variables $d_1$ and $d_2$, which when optimized provides the best positioning of the two bridges to maximize the density of foraging ants on the trail.

A straightforward extension of the two bridge case leads to the following model for a situation such as illustrated in Fig. 5, that may lead to the formation of three bridges. In this case we obtain

$$\rho = \frac{N-\frac{n_{b_1}}{\alpha}-\frac{n_{b_2}}{\alpha}-\frac{n_{b_3}}{\alpha}}{f}, \quad (24)$$

with

$$f = L_T + \left(1-\frac{d_1}{D_{\max}}\right)L_{A_1} + \left(1-\frac{d_3}{D_{\max}}\right)L_{A_4} + \left|\frac{D_{\max}-d_1}{\cos\left(\frac{\theta}{2}\right)} - \frac{d_2}{\cos\left(\frac{\theta}{2}\right)}\right| + \left|\frac{D_{\max}-d_2}{\cos\left(\frac{\theta}{2}\right)} - \frac{d_3}{\cos\left(\frac{\theta}{2}\right)}\right| + b_1 + b_2 + b_3, \quad (25)$$

and with the bridge lengths and the number of ants sequestered for bridge formation given by the same expressions as in the two bridge case.

A term of the form

$$\left|\frac{D_{\max}-d_i}{\cos\left(\frac{\theta}{2}\right)} - \frac{d_{i+1}}{\cos\left(\frac{\theta}{2}\right)}\right| \quad (26)$$

such as appears in Eqs. (23) and (25) is called the **mid-distance** between two consecutive bridges. The mid-distance measures the linear distance between two consecutive bridges along a common arm of an apparatus. The mid-distance serves as a convenient quantity for measuring where two or more bridges form relative to one another. In the results, we plot the mid-distance for optimal bridge position as a function of apex angle in order to visualize that the optimal positioning of two or more bridges seems to be coordinated in a particular manner.

We note that each of the density functions (Eqs. (11), (19), and (24)) is guaranteed to have a biologically relevant maximum

**Table 4**
Geometric parameters and variables corresponding to three-ape apparatus such as shown in Fig. 5.

| Notation | Description | Value | Units |
|---|---|---|---|
| $L_0$ | Hinge-to-hinge length of each arm | 22 | cm |
| $\theta$ | Angle of each apex | 0 to 60 | degrees |
| $w_\theta$ | Ratio between width and length of a bridge, value from Reid et al. (2015) | $4.799\theta^{-0.5014}$ | N/A |
| $L_{A_1}$, $L_{A_2}$, $L_{A_3}$, $L_{A_4}$ | Travel length along each arm of apparatus from apex to opposite hinge | $L_0 - \frac{w_A}{2}\cot\left(\frac{\theta}{2}\right)$ | cm |
| $L_A$ | Sum of travel lengths along each arm | $L_{A_1} + L_{A_2} + L_{A_3} + L_{A_4}$ | cm |
| $D_{\max}$ | Maximum vertical distance from apex to end of each arm | $\frac{L_A}{4}\cos\left(\frac{\theta}{2}\right)$ | cm |
| $d_1$ | Vertical distance of bridge from apex to position on arms forming first apex | 0 to $D_{\max}$ | cm |
| $d_2$ | Vertical distance of bridge from apex to position on arms forming second apex | 0 to $D_{\max}$ | cm |
| $d_3$ | Vertical distance of bridge from apex to position on arms forming third apex | 0 to $D_{\max}$ | cm |

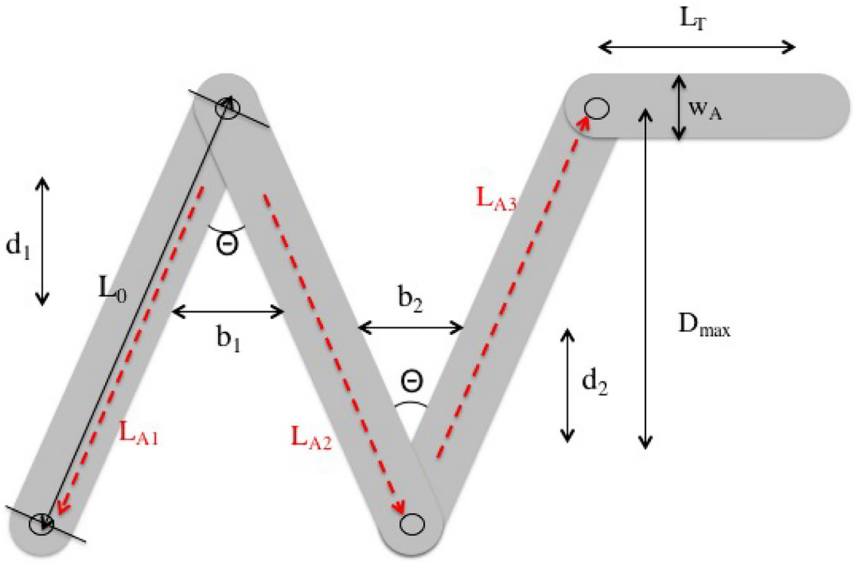


**Fig. 4.** Schematic of a theoretical apparatus that is predicted to result in the construction of two distinct army ant living bridges. The additional linear length of such an apparatus added to the path of travel is well-approximated by $L_A = L_{A_1} + L_{A_1} + L_{A_1}$. Note that, due to symmetry $L_{A_1} = L_{A_2} = L_{A_3}$. All other variables and parameters are described in Tables 1 and 3.

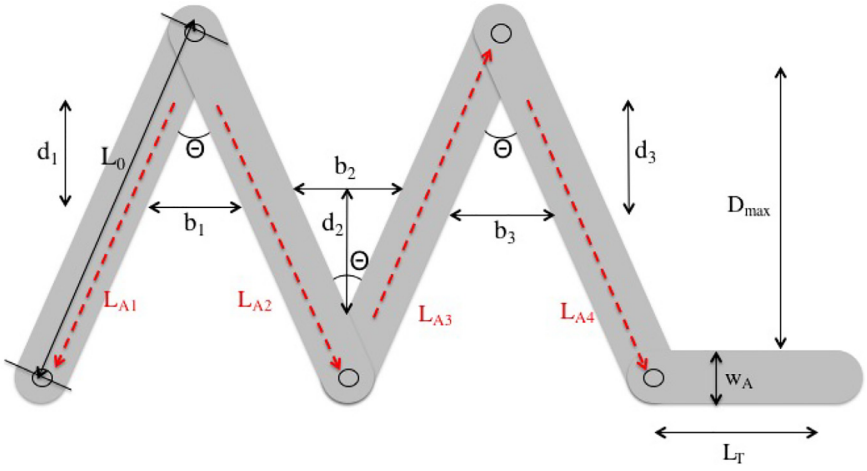


**Fig. 5.** Schematic of a theoretical apparatus that is predicted to result in the construction of three distinct army ant living bridges. The additional linear length of such an apparatus added to the path of travel is well-approximated by $L_A = L_{A_1} + L_{A_2} + L_{A_3} + L_{A_4}$. Note that, due to symmetry, $L_{A_1} = L_{A_2} = L_{A_3} = L_{A_4}$. All other variables and parameters are described in Tables 1 and 4.

value since it is a continuous function maximized over a closed and bounded set of possible distance values. However, unlike in Reid et al. (2015), the presence of square roots, *e.g.*, in (10), and absolute values, *e.g.*, in (25), make the equations much less tractable to solving analytically for exact expression for optimal bridge-positioning. Additional discussion of this and some related points are provided in the appendix.

### 2.5. Model parameters

In order to solve these models, we choose parameter values that are either taken directly from Reid et al. (2015), or chosen to be consistent with values from Reid et al. (2015). Specifically, for the lengths of the sides of a proposed apparatus, we choose parameter values that are on the order of the lengths of the

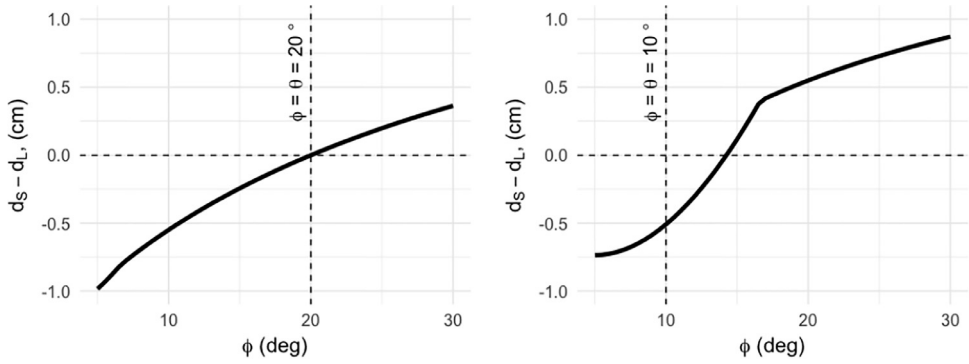


(a) $\theta = 20°$ (b) $\theta = 10°$

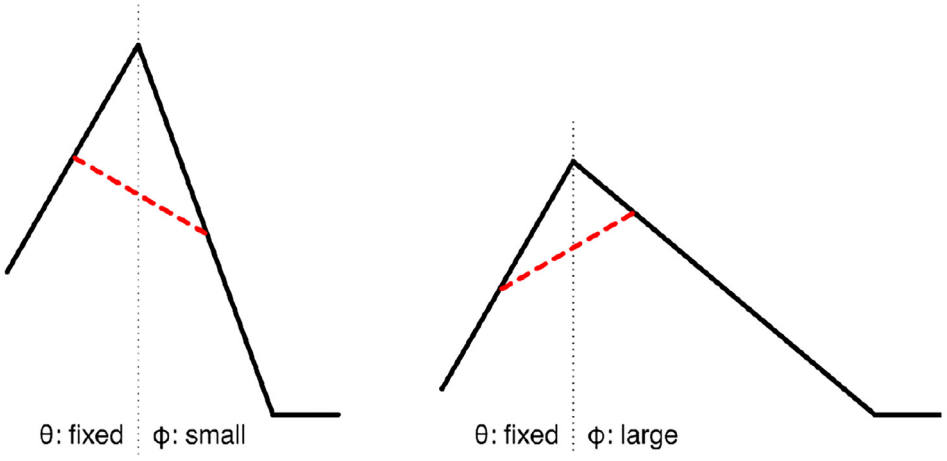


(c)

**Fig. 6.** Quantitative (6(a) - 6(b)) and qualitative (6(c)) results described in Section 3.1. These results show the predicted arrangement of optimal living bridge configurations for an asymmetric apparatus as a function of the angle $\phi$ with the angle $\theta$ fixed at 20° (6(a)) and 10° (6(b)) respectively. Eq. (61) implies that a living bridge forms at the apex of the apparatus and quickly establishes an angle with respect to the main trail axis that is completely determined by the ratio $\frac{\cos(\theta)}{\cos(\phi)}$. This angle with respect to the main trail remains constant as the living bridge moves down the apparatus to its equilibrium position, at least until the bridge "runs out of road" along one arm or the other. That is, for fixed $\theta$ and $\phi$, the orientation of the living bridge only changes as the bridge moves down the apparatus if it reaches the bottom of the shorter side before establishing its equilibrium position. Computed for a foraging density of approximately 2.2.

experimental apparatus from Reid et al. (2015). The values for all parameters used to obtain the following results are listed in Tables 1–4. However, the theory does not depend on the explicit values of the geometric parameters. Therefore, our approach can be adapted to the specific measurements of a different experimental apparatus or naturally occurring obstacles.

### 2.6. Model code

As part of supplementary material, we have developed freely available code using the R programming language, R Core Team (2016), that can be used to implement the models from this paper or any similar models that one may derive. This package can be found at https://goo.gl/zam27s.

## 3. Results and discussion

### 3.1. Asymmetric scenario

In general, optimal bridges in asymmetric apparatuses are not parallel to the main trail axis. Examples of optimal bridge positions are illustrated in Fig. 6a and b. To obtain these results, we fixed one of the arm angles, $\theta$, to be either 20° or 10°, and varied the other angle, $\phi$, from 5° to 30°. We then calculated the optimal bridge position for each combination of angles as the maximizing distances,[2] $d_S$ and $d_L$, that the two ends of the optimal bridge travel down each arm of the apparatus from the apex (Fig. 3), and plotted the difference between these two lengths. Here, a negative difference indicates that the optimal bridge travels further down the arm associated with the angle $\phi$ (here, the longer arm), whereas a positive difference indicates that the bridge travels further down the arm associated with the angle $\theta$ (the shorter arm).

Typically, the optimal bridge travels further down the apparatus arm with a smaller angle (Fig. 6a). This is shown by the difference in bridge end positions being negative when $\phi < \theta$ and positive when $\phi > \theta$. Specifically, we find as derived in the appendix that

$$d_S = \frac{\cos(\theta)}{\cos(\phi)} d_L. \tag{27}$$

This relationship implies that when the two angles $\phi$ and $\theta$ are equal, the optimal bridge tends to be parallel to the main trail axis. Therefore, the symmetric experimental apparatus studied in

[2] Although a slight abuse of notation, throughout Section 3 we use $d_S$, etc. to denote not variables, but the value of the distance variables that actually maximize the relevant density function $\rho$.

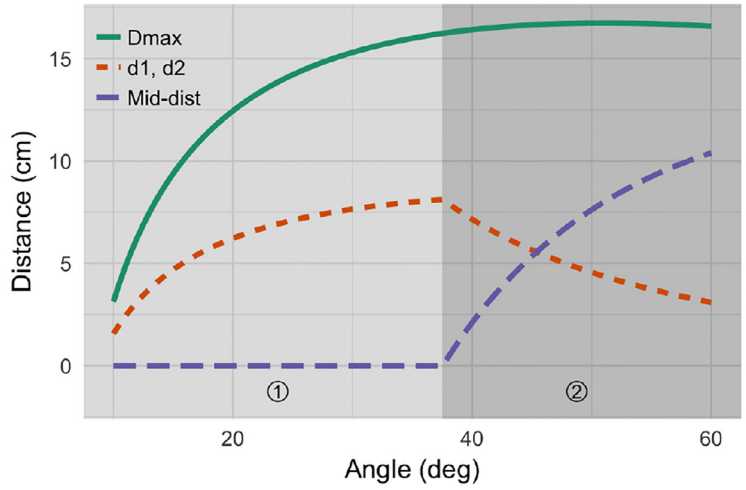


(a)

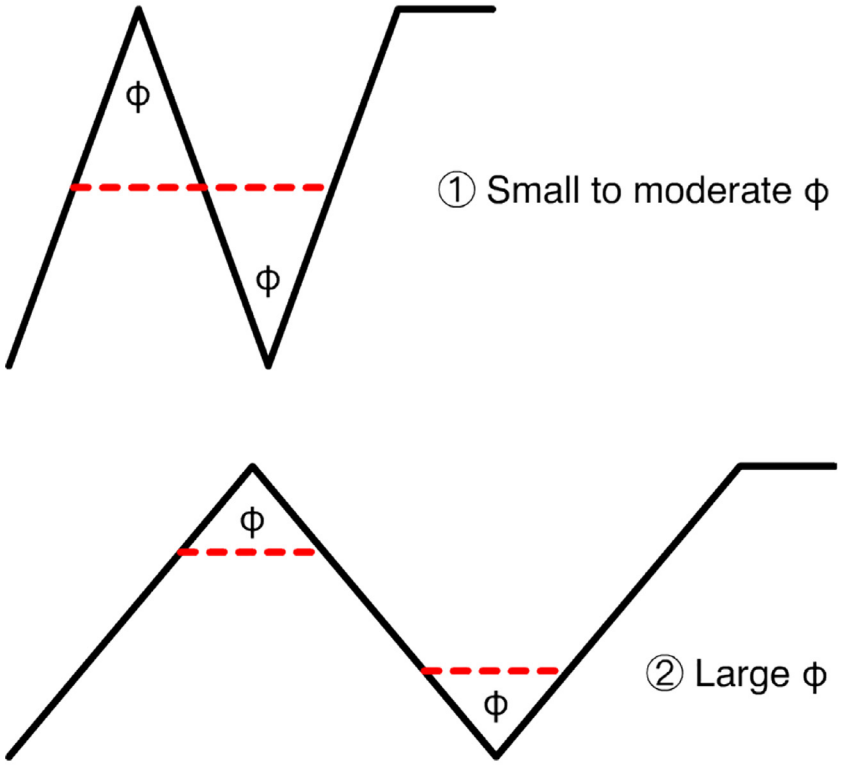


(b)

**Fig. 7.** Fig. 7a shows, as a function of angle $\theta$, the greatest possible vertical distance a living bridge can travel along an apparatus, the distance values $d_1$ and $d_2$ that optimize the density function (19) and determine the optimal positioning of a living bridge, and the mid-distance between two bridges, as defined by formula (26), at their optimal positioning. We plot the mid-distance in order to visualize that the optimal positioning of two or more bridges seems to be coordinated in a particular manner. Thus, the theory predicts that optimal bridge formation for an apparatus such as Fig. 4 is such that the linear distance between two bridges along a common arm is minimized as much as the availability of bridge-building ants allows for under the given geometric constraints imposed by apex angle. For the quantitative results presented here, a foraging density value of approximately 2.2 is used. Qualitatively similar results are obtained for a variety of different parameter values.

Reid et al. (2015) is shown to be a special case of the more general asymmetric apparatus.

However, when the angle $\theta$ is small, we observe deviations from the above behavior. In this case, bridges parallel to the main trail axis can form even when the two angles are not equal (Fig. 6b). When the two angles are equal, the bridge is skewed such that it is further down the arm associated with the angle $\phi$ (the longer arm). This is due to the unequal lengths of the two arms of the apparatus (Fig. 3). The arm associated with the angle $\theta$ is shorter than that associated with angle $\phi$, and the arm lengths define the maximum distance that the bridge can travel. In this regime, one end of the bridge meets the maximum distance of the shorter arm, but the other end continues to travel further down the longer arm. This phenomenon also explains the presence of a 'kink' in the curve in Fig. 6b.

Nonetheless, the trend that the difference in distance increases as the angle $\phi$ increases is still observed, such that a similar transition from a negative difference to a positive difference occurs,

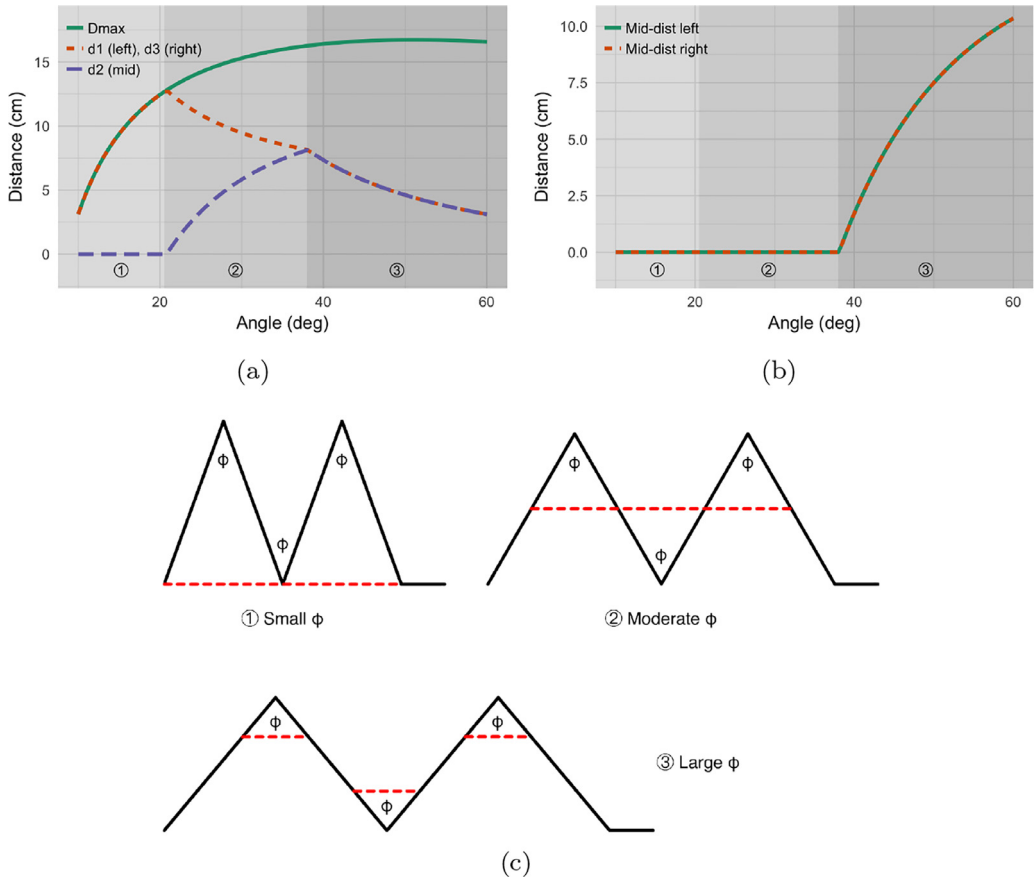


**Fig. 8.** Fig. 8a shows, as a function of angle $\theta$, the greatest possible vertical distance a living bridge can travel along an apparatus and the distance values $d_1$, $d_2$, and $d_3$ that optimize the density function (24) and determine the optimal positioning of a living bridge. Fig. 8b shows the mid-distance, as defined by formula (26), between two consecutive bridges at their optimal positioning. Thus, the theory predicts that optimal bridge formation for an apparatus such as Fig. 5 is such that the linear distance between all three bridges along common arms is minimized as much as the availability of bridge-building ants allows for under the given geometric constraints imposed by apex angle. For the quantitative results presented here, a foraging density value of approximately 2.2 is used. Qualitatively similar results are obtained for a variety of different parameter values.

albeit when $\phi > \theta$. Therefore, in general we predict bridges to travel further down the arm associated with angle $\phi$ when $\phi$ is small, and travel further down the arm associated with angle $\theta$ when $\phi$ is large. This prediction holds as parameters are varied and for a wide range of angles.

We can predict not only the optimal final position of a living bridge, but also the optimal bridge formation process, by constraining the bridge length to certain values shorter than the final length and solving for the optimal bridge at each length (the appendix contains the details of solving this constrained optimization problem). Because Eq. (27) is true for any bridge length, it predicts that a living bridge forms at the apex of the apparatus and immediately establishes an angle with respect to the main trail axis that is completely determined by the ratio $\frac{\cos(\theta)}{\cos(\phi)}$. This angle with respect to the main trail remains constant as the living bridge moves down the apparatus to its equilibrium position, at least until the bridge "runs out of road" along one arm or the other. That is, for fixed $\theta$ and $\phi$, the orientation of the living bridge only changes as the bridge moves down the apparatus if it reaches the bottom of the shorter side before establishing its equilibrium position.

### 3.2. Multiple obstacles scenario

When there are multiple obstacles, we find that multiple bridges form, although, as with asymmetric obstacles, the position of the bridges depends on the angle of the apparatus (Figs. 7 and 8). For the case of two obstacles (7), small and moderate angles result in optimal bridges which are situated halfway between the two apexes, such that the two bridges form a straight path. In this regime, as the angle of the apparatus increases, the maximal possible distance that a bridge can move from the apex, $D_{\max}$, increases, and both bridges have distance $\frac{D_{\max}}{2}$ from each apex (note that $D_{\max}$ increases, rather than decreases, with the apparatus angle because of the nonzero width of the apparatus arm, see Methods and Reid et al., 2015). Furthermore, the distance between the two bridges remains 0. At large angles, however, the bridges are predicted to separate and move closer to their respective apex as the angle increases further. This is illustrated by the distance of the two bridges from the apex decreasing and the distance between the two bridges increasing.

For the case of three obstacles, there are three, rather than two regimes (Fig. 8). For small apparatus angles, only two bridges form, which together extend the main trail axis in a straight line. Here, as the angle increases, the maximum possible distance from the apexes ($D_{\max}$) increases, and the outer bridges remain at the maximum distance $d_1 = d_2 = D_{\max}$, while the inner bridge has zero length. For moderate angles, there are three bridges, which together form a straight line. As the angle increases in this regime, the bridges move increasingly toward the middle of the apparatus. At large angles, the three bridges separate, as in the two-obstacle case, and all three bridges have equal length. As the apparatus angle increases further, each bridge moves towards its respective apex.

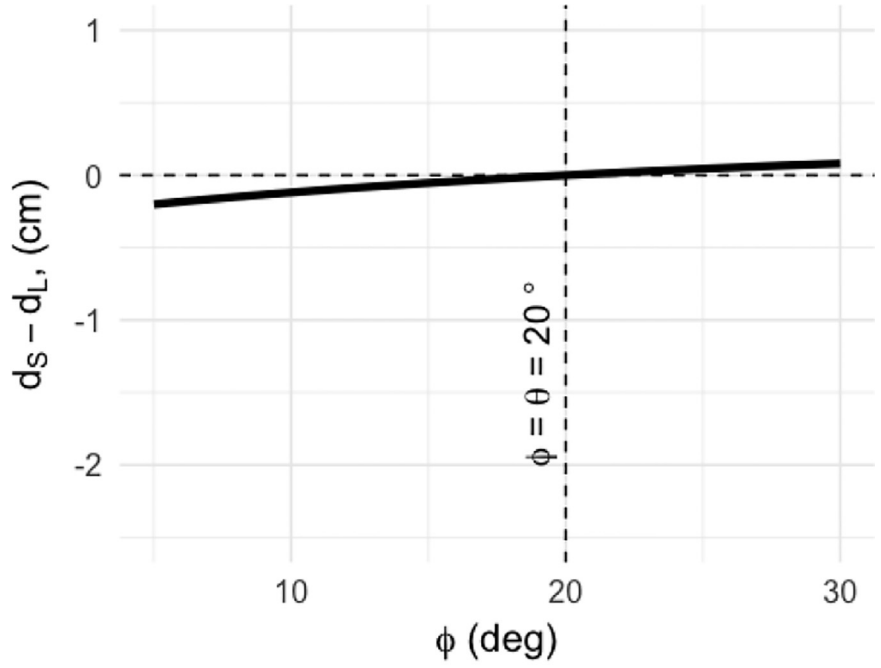


(a) foraging density = 0.5

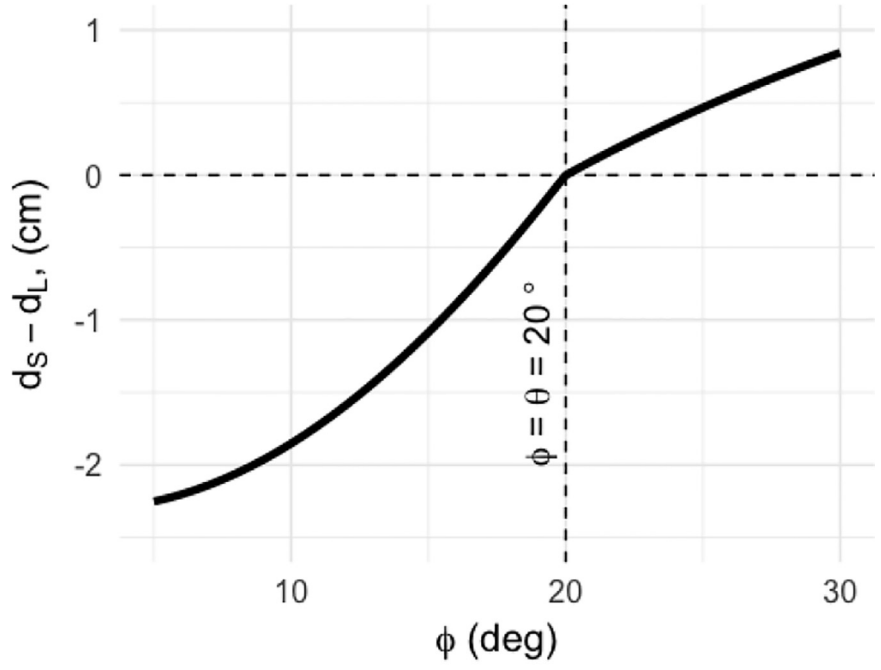


(b) foraging density = 5.0

**Fig. 9.** In nature, the density of ants on a trail can vary dramatically. Motivated by this, we investigated how ant density affects our previous results. For example, we compare the quantitative results as shown in Fig. 9a with those obtained by decreasing (9 a) and increasing (9 b) the density. In general, the effects of changing the angle of the apparatus become more larger as ant density increases. However, the qualitative features of our results remain the same across densities. The situation is highly similar for the other apparatus configurations considered in this work. Thus, the predictions made by the theory are robust with respective to the qualitative behavior predicted.

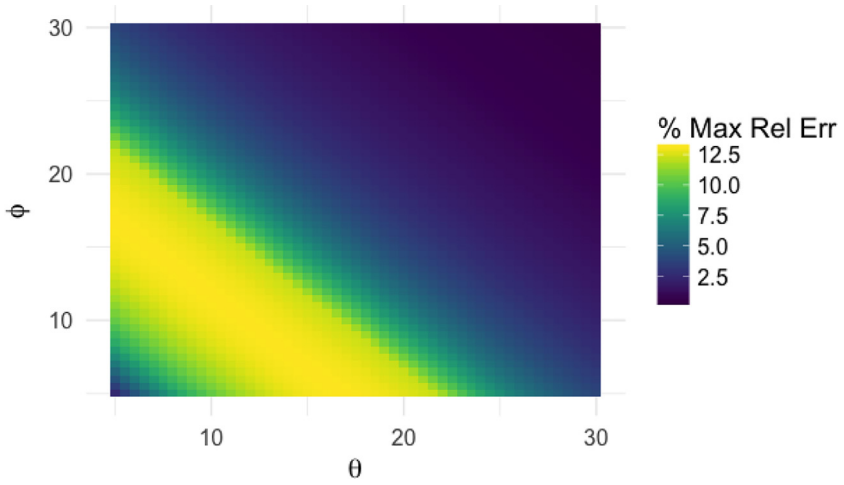


**Fig. 10.** Figure shows the percent maximum relative error as defined in Section 3.4 for the asymmetric apparatus model. Figures such as this provide an approach for experimentalists to determine how close observed densities corresponding to a living bridge configuration are to those predicted to be optimal by the theoretical models for various apex angles. We promote parameter domains that lead to higher percent maximum relative error as favorable regions for an experimentalist to target since there the cost of deviating from the optimal position is relatively high.

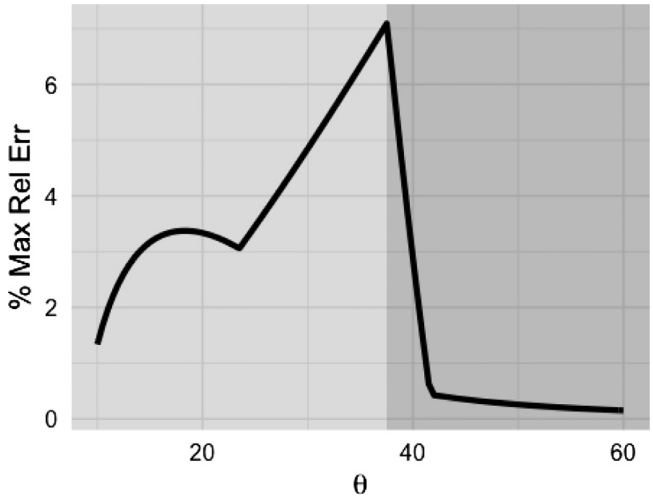


**Fig. 11.** Figure shows the percent maximum relative error as defined in Section 3.4 for the two-apex apparatus model. Figures such as this provide an approach for experimentalists to determine how close observed densities corresponding to a living bridge configuration are to those predicted to be optimal by the theoretical models for various apex angles. Locations of dramatic changes in the percent relative error closely align with those of the results from Fig. 7a. We promote parameter domains that lead to higher percent maximum relative error as favorable regions for an experimentalist to target since there the cost of deviating from the optimal position is relatively high.

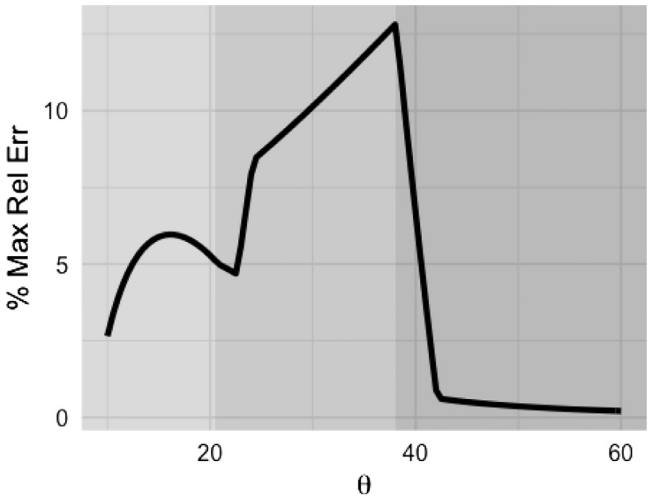


**Fig. 12.** Figure shows the percent maximum relative error as defined in Section 3.4 for the three-apex apparatus model. Figures such as this provide an approach for experimentalists to determine how close observed densities corresponding to a living bridge configuration are to those predicted to be optimal by the theoretical models for various apex angles. Locations of dramatic changes in the percent relative error closely align with those of the results from Fig. 8a. We promote parameter domains that lead to higher percent maximum relative error as favorable regions for an experimentalist to target since there the cost of deviating from the optimal position is relatively high.

### 3.3. The role of ant density

In nature, the density of ants on a trail can vary dramatically, depending on the time of day, the size of the colony, and the amount of available food in the trail's vicinity. We investigated how ant density affects our previous results. We show results for the asymmetric apparatus, although we find qualitatively similar results for the two-obstacle and three-obstacle scenarios.

In general, the effects of changing the angle of the apparatus become larger as ant density increases (Fig. 9a and b). However, the qualitative features of our results remain the same across densities. Thus, performing experiments on trails with higher densities of ants will improve the ability to detect the patterns of bridge formation that we predict, if ants build bridges in order to maximize foraging rate as hypothesized in Reid et al. (2015).

### 3.4. Comparison with experimental observations

We now describe an approach for comparing our theoretical predictions with future experimental results. Specifically, we examine how much variation is possible, in terms of the relative error, for the density when compared with the predicted maximized density whenever the army ant living bridge position is allowed to deviate up to 25% from the position that is predicted to maximize the density. Let $\rho_{\max}$ be the optimized density, then

$$\%\text{Rel Err} = \frac{\rho_{\max} - \rho}{\rho_{\max}} \times 100, \tag{28}$$

specifies the percent relative error. Since in our model the density $\rho$ is a function of the position of living bridges, we allow the positions of any living bridges to deviate up to 25% from the position that is predicted to maximize the density, and then compute the

maximum of all possible relative error (29) within this range. That is, for fixed apparatus apex angles let $S$ denote the set of all bridge positions that lie within 25% of the position that maximizes the density $\rho$, then we define

$$\%\text{Max Rel Err} = \max_{S} \frac{\rho_{\max} - \rho}{\rho_{\max}} \times 100, \tag{29}$$

Furthermore, we carry out this procedure for each of the apparatus apex angles considered in the results presented in the last section. We note that we choose a deviation of up to 25% from the predicted optimal position since it consistently leads to percent relative error values around or below 10%-15% which should be an acceptable range for the relevant types of experiments.

Figs. 10–12 display the outcome of the procedure just described to the asymmetric, two-bridge, and three-bridge scenarios respectively. We promote parameter domains that lead to higher percent maximum relative error as favorable regions for an experimentalist to target since there the cost of deviating from the optimal position is relatively high. Essentially, the results presented in Figs. 10–12 provide guides to an experimenter for parameter ranges where we expect observed bridges to more closely match the predicted optimal bridges. Additionally, they also give a new prediction that can be tested by experimenters: in high max relative error regions, we expect smaller variations in bridge configuration across repeated trials, while in low max relative error regions, we expect greater variation.

## 4. Conclusion

Determining the details of the construction of army ant living bridges is important to understanding the collective behavior of army ants. We extended a mathematical model for a specific case living bridge construction into a broad theoretical framework that may be applied to a variety of increasingly complex natural and experimental obstacles, which are predicted to result in the formation of a living bridge by foraging army ants. Using this framework, we made explicit predictions that can be experimentally tested. In particular, for each scenario, we identified qualitatively different bridge-building regimes, depending on the configuration of the experimental apparatus, which will be more amenable to testing in the field. If the living bridges that army ants construct function mainly to maximize foraging rate, then these different regimes will be observed in nature.

## Acknowledgments

ABK is supported by a James S. McDonnell Foundation Postdoctoral Fellowship Award in Studying Complex Systems. DAW's effort was supported through the Mathematical Biosciences Institute's Research Experience for Undergraduates Program (NSF DMS - 1461163).

## Appendix

In this appendix, we expound additional properties of the theory presented in the main body of this work by carrying out a more detailed mathematical analysis of density functions such as the one from Reid et al. (2015) and those of Eqs. (11) and (19). We note that in the interest of mathematical generality, in this appendix we adopt slightly different notation than is used in Reid et al. (2015) and Section 2.

We begin with the observation that the density function (3) applied to the configuration from Reid et al. (2015) can be written as

$$\rho(x) = \frac{\mathcal{N}(x)}{f(x)} = \frac{ax^2 + b}{px + q}, \tag{30}$$

where $a$, $b$, $p$, $q$ are parameters. The biological interpretation of Eq. (30) is that the quadratic function $\mathcal{N}(x) = ax^2 + b$ describes the relevant number of ants while the linear function $f(x) = px + q$ describes the relevant linear distance of travel. The only *a priori* assumption that we place on the coefficients $a$, $b$, $p$, $q$ is that $p$, $q$ must be chosen so that $f(x) = px + q$ is positive for all biologically reasonable values of the independent variable $x$. As discussed in Reid et al. (2015), the fact that $\mathcal{N}(x)$ is quadratic, while $f(x)$ is linear and positive is a key point of the cost-benefit trade-off aspect of the theory of army ant living bridge formation.

We proceed with our analysis by computing the first and second derivatives of (30) with respect to the independent variable $x$ thus obtaining

$$\rho'(x) = \frac{apx^2 + 2aqx - pb}{(px + q)^2}, \tag{31}$$

$$\rho''(x) = \frac{2(aq^2 + bp^2)}{(px + q)^3}. \tag{32}$$

Now we seek to determine conditions under which Eq. (30) is maximized for a unique positive value $x^* \in [0, M]$, where $M$ represents the maximum possible distance value. Thus, we seek to determine a positive value of $x$ in the interval $[0, M]$ such that $\rho'(x) = 0$ and $\rho''(x) < 0$. Using the assumption that $f(x) = px + q$ is positive for all biologically reasonable values of the independent variable $x$, this will happen whenever $apx^2 + 2aqx - pb = 0$ and $aq^2 + bp^2 < 0$, and therefore whenever $x^*$ satisfies

$$0 < x^* = -\frac{q}{p} + \sqrt{\left(\frac{q}{p}\right)^2 - \frac{b}{a}} \leq M, \tag{33}$$

and

$$\frac{b}{a} < -\left(\frac{q}{p}\right)^2. \tag{34}$$

Note that in order to obtain a positive maximizing value of $x$ in the interval $[0, M]$, it must be the case that $\frac{b}{a} < 0$.

Conditions (33) and (34) can easily be used to recover the results on optimal bridge positioning from Reid et al. (2015). The benefit of the different approach taken here is that it is applicable in situations not necessarily covered by the analysis of Reid et al. (2015), provided that the configuration is such that the positioning of the army ant living bridge is completely determined by a single distance variable $x$. More interestingly, the analysis just given suggests how to move to multi-variable problems via analogy.

Consider the two-variable function

$$\rho(x, y) = \frac{\mathcal{N}(x, y)}{f(x, y)} = \frac{ax^2 + bxy + cy^2 + d}{px + qy + r}, \tag{35}$$

where now the only assumptions on the parameters $a$, $b$, $c$, $d$, $p$, $q$, $r$ is that $p$, $q$, $r$ are such that $f(x) = px + qy + r$ is positive for all biologically reasonable values of the independent variables $x$, $y$. We note two points regarding Eq. (35): While we restrict our analysis to the two-variable case for notational simplicity, our work makes clear how to proceed in cases of three or more variables. More importantly, while (35) is similar in form to Eqs. (11) and (19) of Section 2; it is only locally equivalent due to the presence of the square root in (10) and the absolute value in (23). Nevertheless, an analysis of (35) still provides valuable insight into the results we obtain from Eqs. (11) and (19), namely it aids in the explanation for the symmetry of the results derived from (19).

As before, we proceed with our analysis by computing the first and second derivatives of (35) with respect to the independent variables $x$, $y$ thus obtaining

$$\frac{\partial \rho}{\partial x} = \frac{apx^2 + 2aqxy + (bq - cp)y^2 + 2arx + bry - dp}{(px + qy + r)^2}, \tag{36}$$

$$\frac{\partial \rho}{\partial y} = \frac{(bp - aq)x^2 + 2cpxy + cqy^2 + brx + 2cry - dq}{(px + qy + r)^2}, \tag{37}$$

$$\frac{\partial^2 \rho}{\partial x^2} = \frac{(2aq^2 - 2bpq + 2cp^2)y^2 + (4aqr - 2bpr)y + 2(ar^2 + dp^2)}{(px + qy + r)^3}, \tag{38}$$

$$\frac{\partial^2 \rho}{\partial y^2} = \frac{(2aq^2 - 2bpq + 2cp^2)x^2 + (4cpr - 2bqr)x + 2(cr^2 + dq^2)}{(px + qy + r)^3}, \tag{39}$$

$$\frac{\partial^2 \rho}{\partial x \partial y} = \frac{2(bq - cp^2 - aq^2)xy + r(bp - 2aq)x + r(bq - 2cp)y + 2dq + br^2}{(px + qy + r)^3}. \tag{40}$$

We would again like to find conditions for unique positive values for $x$ and $y$ in intervals $[0, M]$ and $[0, N]$ respectively that maximize the function (35)). In general, the complexity of the expressions in Eqs. (36)–(40) make solving explicitly for maximizing values of $x$ and $y$ difficult. However, there are simplifying assumptions that can be made that are relevant to the multi-bridge configurations studied in Section 2, that is, the case whenever $b = 0$, $a = c$, and $p = q$. This is in perfect analogy with the density function (19) from Section 2. Under these assumptions, we get

$$\frac{\partial \rho}{\partial x} = \frac{apx^2 + 2apxy - apy^2 + 2arx - dp}{(px + py + r)^2}, \tag{41}$$

$$\frac{\partial \rho}{\partial y} = \frac{-apx^2 + 2apxy + apy^2 + 2ary - dp}{(px + py + r)^2}, \tag{42}$$

$$\frac{\partial^2 \rho}{\partial x^2} = \frac{2(2ap^2y^2 + 2apry + (ar^2 + dp^2))}{(px + py + r)^3}, \tag{43}$$

$$\frac{\partial^2 \rho}{\partial y^2} = \frac{2(2ap^2x^2 + 2aprx + (ar^2 + dp^2))}{(px + py + r)^3}, \tag{44}$$

$$\frac{\partial^2 \rho}{\partial x \partial y} = \frac{-2(2ap^2xy + aprx + apry - dp)}{(px + py + r)^3}, \tag{45}$$

from which one can see that there is a value $t$ satisfying $x = y = t$ and

$$t = -\frac{1}{2}\frac{r}{p} + \frac{1}{2}\sqrt{\left(\frac{r}{p}\right)^2 + 2\frac{d}{a}} \tag{46}$$

so that $\frac{\partial \rho}{\partial x}(t, t) = \frac{\partial \rho}{\partial y}(t, t) = 0$. That is, there is a symmetric critical point for Eq. (35). Moreover, it is easy to see that when evaluated at $(t, t)$ we have

$$D = \frac{\partial^2 \rho}{\partial x^2}\frac{\partial^2 \rho}{\partial y^2} - \left(\frac{\partial^2 \rho}{\partial x \partial y}\right)^2 > 0. \tag{47}$$

Thus, if $2ap^2t^2 + 2aprt + ar^2 + dp^2 < 0$, then the symmetric critical point $(t, t)$ is at least a local maximum for (35). In addition, one can conclude from (46) when $t$ will be in an interval of the form $[0, M]$. This analysis aids in our understanding of the symmetry of the results summarized in Fig. 7b obtained for the optimal bridge-position in the two-bridge configuration such as illustrated by Fig. 4. Similar reasoning for three independent variables can help to explain the symmetric results for the three-bridge configuration.

Now, we derive the results for the constrained optimization problem described in Section 3. Specifically, we derive what is predicted to happen when the overall living bridge length is interpreted as a parameter. Doing so provides insight into the process of optimal bridge formation. Let $b_f$ represent the bridge length parameter. When $b_f$ is fixed, through Eqs. (9)–(11) we arrive at a constrained optimization problem. That is, we seek to optimize the density

$$\rho = \frac{N - \frac{n_{b_f}}{\alpha}}{f}, \tag{48}$$

subject to the constraint

$$b_f^2 = \left(\frac{L_{A,S}}{D_{\max,1}}d_1\right)^2 + \left(\frac{L_{A,L}}{D_{\max,2}}d_2\right)^2 - 2d_1d_2\frac{L_{A,S}L_{A,L}\cos(\theta + \phi)}{D_{\max,1}D_{\max,2}}, \tag{49}$$

where

$$f = L_T + L_A + b_f - \frac{L_{A,S}}{D_{\max,1}}d_1 - \frac{L_{A,L}}{D_{\max,2}}d_2, \tag{50}$$

and

$$n_{b_f} = \frac{w_\Omega\left(1 - w_\Omega \tan\left(\frac{\theta + \phi}{2}\right)\right)}{l_n w_n}b_f^2. \tag{51}$$

We note that $n_{b_f}$ and hence $N - \frac{n_{b_f}}{\alpha}$ are now held constant. The values for $L_{A,S}$, $L_{A,L}$, $D_{\max,1}$ and $D_{\max,2}$ are obtained just as before.

Examining Eqs. (48) and (49) we see that we need to maximize a function of the form

$$\rho(x, y) = \frac{\mathcal{N}}{A - px - qy}, \tag{52}$$

subject to a constraint of the form

$$g(x, y) = p^2x^2 + q^2y^2 - 2pqCxy = k^2, \tag{53}$$

where $\mathcal{N}$, $A$, $k$, $p$, $q$ and $C$ are parameters. To simplify the problem, we observe that maximizing (52) subject to (53) is equivalent to minimizing $f(x, y) = A - px - qy$ subject to the same constraint. This is done in a straightforward manner using the method of Lagrange multipliers. That is, we solve

$$-p = \lambda(2p^2x - 2pqCy), \tag{54}$$

$$-q = \lambda(2q^2y - 2pqCx), \tag{55}$$

$$k^2 = p^2x^2 + q^2y^2 - 2pqCxy, \tag{56}$$

for $\lambda$, $x$ and $y$ that minimize $f(x, y) = A - px - qy$. This is easily done using (54) and (55) to set $px - qCy = qy - pCx$ and then substituting into (56) and solving for the remaining variable. This gives solution

$$x = \frac{k}{p}\sqrt{\frac{1}{2(1 - C)}}, \tag{57}$$

$$y = \frac{k}{q}\sqrt{\frac{1}{2(1 - C)}}, \tag{58}$$

where we have retained only the positive square roots since in our application we seek positive distance values. Setting $k = b_f$, $p = \frac{L_{A,S}}{D_{\max,1}}$, $q = \frac{L_{A,L}}{D_{\max,2}}$ and $C = \cos(\theta + \phi)$

$$d_1 = \frac{D_{\max,1}}{L_{A,S}}\sqrt{\frac{1}{2(1 - \cos(\theta + \phi))}}b_f, \tag{59}$$

$$d_2 = \frac{D_{\max,2}}{L_{A,L}}\sqrt{\frac{1}{2(1 - \cos(\theta + \phi))}}b_f. \tag{60}$$

Keep in mind that we must set $d_i = D_{\max,i}$ if $b_f$ is such that the predicted value of either $d_1$ or $d_2$ is greater than or equal to $D_{\max,1}$ or $D_{\max,2}$ respectively. Furthermore, using the expressions (7) and (8) together with Eqs. (59) and (60), we see that the ratio of optimal distance values $d_1$ and $d_2$ satisfies

$$\frac{d_1}{d_2} = \frac{\cos(\theta)}{\cos(\phi)}. \tag{61}$$

From this equation we can deduce interesting predictions. In particular, rearranging Eq. (61) gives

$$d_1 = \frac{\cos(\theta)}{\cos(\phi)} d_2. \tag{62}$$

The biological consequences of this are described in Section 3.1.

## References


Anderson, C., Theraulaz, G., Deneubourg, J.-L., 2002. Self-assemblages in insect societies. Insectes Soc. 49 (2), 99–110. ISSN 0020-1812. doi: 10.1007/s00040-002-8286-y.

Ardia, D., Arango, J.O., Gomez, N.G., 2011. Jump-diffusion calibration using differential evolution. Wilmott Mag. 55, 76–79. URL http://www.wilmott.com/.

Ardia, D., Boudt, K., Carl, P., Mullen, K.M., Peterson, B.G., 2011. Differential evolution with DEoptim: an application to non-convex portfolio optimization. R J 3 (1), 27–34. URL http://journal.r-project.org/archive/2011-1/2011-1_index.html.

Ardia, D., Mullen, K. M., Peterson, B. G., Ulrich, J., 2015. DEoptim: Differential Evolution in R. Version 2.2–3, URL http://CRAN.R-project.org/package=DEoptim.

Berdahl, A., Torney, C.J., Ioannou, C.C., Faria, J.J., Couzin, I.D., 2013. Emergent sensing of complex environments by mobile animal groups. Science 339 (6119), 574–576. ISSN 0036-8075,URL http://science.sciencemag.org/content/339/6119/574.

Bochynek, T., Meyer, B., Burd, M., 2016. Energetics of trail clearing in the leaf-cutter ant atta. Behav. Ecol. Sociobiol. 71 (1), 14. ISSN 0340-5443, 1432-0762, URL http://link.springer.com/article/10.1007/s00265-016-2237-5.

Bruce, A.I., Burd, M., 2012. Allometric scaling of foraging rate with trail dimensions in leaf-cutting ants. Proc. R. Soc. B 279 (1737), 2442–2447. ISSN 1471-2954, URL http://www.ncbi.nlm.nih.gov/pubmed/22337696.

Buhl, J., Deneubourg, J.-L., Grimal, A., Theraulaz, G., 2005. Self-organized digging activity in ant colonies. Behav. Ecol. Sociobiol. 58 (1), 9–17. ISSN 0340-5443, URL http://www.springerlink.com/index/10.1007/s00265-004-0906-2.

Camazine, S., Deneubourg, J.-L., Franks, N.R., Sneyd, J., Theraulaz, G., Bonabeau, E., 2001. Self-Organization in Biological Systems. Princeton University Press, Princeton, NJ. ISBN 9780691116242

Couzin, I.D., 2009. Collective cognition in animal groups. Trends Cogn. Sci. 13 (1), 36–43. ISSN 1364-6613,URL http://www.ncbi.nlm.nih.gov/pubmed/19058992.

Couzin, I.D., Krause, J., 2003. Self-organization and collective behavior in vertebrates. Adv. Study Behav. 32, 1–75. ISSN 0065-3454, URL http://www.sciencedirect.com/science/article/pii/S0065345403010015.

Couzin, I.D., Krause, J., Franks, N.R., Levin, S.A., 2005. Effective leadership and decision-making in animal groups on the move. Nature 433 (7025), 513–516. ISSN 0028-0836, 1476-4687, URL http://www.nature.com/nature/journal/v433/n7025/abs/nature03236.html.

Cross, P.C., Cole, E.K., Dobson, A.P., Edwards, W.H., Hamlin, K.L., Luikart, G., Middleton, A.D., Scurlock, B.M., White, P.J., 2010. Probable causes of increasing brucellosis in free-ranging elk of the Greater Yellowstone Ecosystem. Ecol. Appl. 20 (1), 278–288. ISSN 1939-5582, URL https://doi.org/10.1890/08-2062.1.

Deneubourg, J.-L., Aron, S., Goss, S., Pasteels, J.M., 1990. The self-organizing exploratory pattern of the argentine ant. J. Insect. Behav. 3 (2), 159–168. ISSN 0892-7553, URL http://www.springerlink.com/index/L76621W5417109QQ.pdf.

Detrain, C., Deneubourg, J.-L., 2006. Self-organized structures in a superorganism: do ants “behave” like molecules? Phys. Life Rev. 3 (3), 162–187. ISSN 1571-0645, URL http://www.sciencedirect.com/science/article/pii/S1571064506000200.

Devigne, C., Detrain, C., 2002. Collective exploration and area marking in the ant Lasius niger. Insectes Soc. 49 (4), 357–362. ISSN 0020-1812, URL http://www.springerlink.com/index/qpern5ccjkld2d5e.pdf.

Duarte, A., Weissing, F.J., Pen, I., Keller, L., 2011. An evolutionary perspective on self-organized division of labor in social insects. Annu. Rev. Ecol. Evol. Syst. 42 (1), 91–110. ISSN 1543-592X, URL https://doi.org/10.1146/annurev-ecolsys-102710-145017.

Garnier, S., Gautrais, J., Theraulaz, G., 2007. The biological principles of swarm intelligence. Swarm Intell. 1 (1), 3–31. ISSN 1935-3812, 1935-3820, URL http://link.springer.com/article/10.1007/s11721-007-0004-y.

Garnier, S., Murphy, T., Lutz, M., Hurme, E., Leblanc, S., Couzin, I.D., 2013. Stability and responsiveness in a self-organized living architecture. PLoS Comput. Biol. 9 (3), e1002984.

Guttal, V., Couzin, I.D., 2010. Social interactions, information use, and the evolution of collective migration. Proc. Natl. Acad. Sci. U.S.A. 107 (37), 16172–16177. ISSN 0027-8424, 1091-6490, URL http://www.pubmedcentral.nih.gov/articlerender.fcgi?artid=2941337&tool=pmcentrez&rendertype=abstract.

Howard, J.J., 2001. Costs of trail construction and maintenance in the leaf-cutting ant atta colombica. Behav. Ecol. Sociobiol. 49 (5), 348–356. ISSN 0340-5443, URL http://link.springer.com/10.1007/s002650000314.

King, H., Ocko, S., Mahadevan, L., 2015. Termite mounds harness diurnal temperature oscillations for ventilation. Proc. Natl. Acad. Sci. U.S.A. 112 (37), 11589–11593. ISSN 0027-8424, 1091-6490, URL https://doi.org/10.1073/pnas.1423242112.

Kost, C., de Oliveira, E.G., Knoch, T.A., Wirth, R., 2005. Spatio-temporal permanence and plasticity of foraging trails in young and mature leaf-cutting ant colonies (atta spp.). J. Trop. Ecol. 21 (06), 677. ISSN 0266-4674, URL http://www.journals.cambridge.org/abstract_S0266467405002592.

Mullen, K., Ardia, D., Gil, D., Windover, D., Cline, J., 2011. DEoptim: An R package for global optimization by differential evolution. J. Stat. Softw. 40 (6), 1–26. URL http://www.jstatsoft.org/v40/i06/.

Powell, S., Franks, N.R., 2005. Caste evolution and ecology: a special worker for novel prey. Proc. R. Soc. Lond. B 272 (1577), 2173–2180. URL http://rspb.royalsocietypublishing.org/content/272/1577/2173.

Powell, S., Franks, N.R., 2006. Ecology and the evolution of worker morphological diversity: a comparative analysis with Eciton army ants. Funct. Ecol. 20 (6), 1105–1114. ISSN 1365-2435, URL https://doi.org/10.1111/j.1365-2435.2006.01184.x.

Powell, S., Franks, N.R., 2007. How a few help all: living pothole plugs speed prey delivery in the army ant eciton burchellii. Anim. Behav. 73 (6), 1067–1076.

Price, K.V., Storn, R.M., Lampinen, J.A., 2006. Differential Evolution - A Practical Approach to Global Optimization. Natural Computing. Springer-Verlag. ISBN 540209506.

R Core Team, 2016. R: A Language and Environment for Statistical Computing. R Foundation for Statistical Computing. Vienna, Austria. URL https://www.R-project.org/.

Reid, C.R., Lutz, M.J., Powell, S., Kao, A.B., Couzin, I.D., Garnier, S., 2015. Army ants dynamically adjust living bridges in response to a cost–benefit trade-off. Proc. Natl Acad. Sci. 112 (49), 15113–15118.

Rettenmeyer, C.W., 1963. Behavioral studies of army ants. estudios de comportamiento de hormigas guerreras. The University of Kansas Science Bulletin. 44 (9), 281–465.

Schneirla, T.C., 1945. The army-ant behavior pattern: nomad-statary relations in the swarmers and the problem of migration. Biol. Bull. 88 (2), 166–193. URL http://www.jstor.org/stable/10.2307/1538043.

Schneirla, T.C., 1972. Army Ants: A Study in Social Organization. W.H. Freeman & Co Ltd.

Solé, R.V., Bonabeau, E., Delgado, J., Fernández, P., Marín, J., 2000. Pattern formation and optimization in army ant raids. Artif. Life 6 (3), 219–226. ISSN 1064-5462, URL http://www.ncbi.nlm.nih.gov/pubmed/11224916.

Sumpter, D.J.T., 2010. Collective Animal Behavior. Princeton University Press, Princeton, NJ. ISBN 9780691129631.

Theraulaz, G., Bonabeau, E., Nicolis, S.C., Solé, R.V., Fourcassié, V., Blanco, S., Fournier, R., Joly, J.-L., Fernández, P., Grimal, A., Dalle, P., Deneubourg, J.-L., 2002. Spatial patterns in ant colonies. Proc. Natl. Acad. Sci. U.S.A. 99 (15), 9645–9649. ISSN 0027-8424, URL http://www.pubmedcentral.nih.gov/articlerender.fcgi?artid=124961&tool=pmcentrez&=abstract.

Wolf, M., Kurvers, R.H.J.M., Ward, A.J.W., Krause, S., Krause, J., 2013. Accurate decisions in an uncertain world: collective cognition increases true positives while decreasing false positives. Proc. Biol. Sci. 280 (1756), 20122777. ISSN 0962-8452, 1471-2954, URL https://doi.org/10.1098/rspb.2012.2777.